Enhanced valence force field model for the lattice properties of gallium arsenide

Sebastian Steiger,* Mehdi Salmani-Jelodar, Denis Areshkin, Abhijeet Paul, Tillmann Kubis, Michael Povolotskyi, Hong-Hyun Park, and Gerhard Klimeck

Network for Computational Nanotechnology, Purdue University, West Lafayette, Indiana 47907, USA

(Received 27 May 2011; revised manuscript received 24 September 2011; published 17 October 2011)

An enhanced valence force field model for zinc-blende crystals is developed to provide a unified description of the isothermal static and dynamical lattice properties of gallium arsenide. The expression for the lattice energy includes a second-nearest-neighbor coplanar interaction term, the Coulomb interaction between partially charged ions, and anharmonicity corrections. General relations are derived between the microscopic force constants and the macroscopic elastic constants in zinc-blende crystals. Applying the model to gallium arsenide, parameter sets are presented that yield quantitative agreement with experimental results for the phonon dispersion, elastic constants, sound velocities, and Grüneisen mode parameters.

DOI: 10.1103/PhysRevB.84.155204 PACS number(s): 73.21.−b

I. INTRODUCTION

The calculation of static and dynamic properties of crystal lattices from atomic configurations has a century-long history.[1] Interest in these quantities is currently revived because of the increasing importance of thermal effects in nanodevices. CPU power consumption, combined with increased resource scarcity, poses serious technological challenges for which the quantitative understanding of nanoscale lattice properties is critical.

A vast variety of models' strain and phonon exist in literature, some of which agree very well with experimentally reported values.[2,3] The empirical valence force field (VFF) approach[4] offers an attractive alternative to more accurate *ab initio* models[3] due to its reduced computational cost and feasibility when it comes to the treatment of systems where thousands, if not millions, of atoms need to be explicitly considered. Yet, many devices are now heavily influenced by interfaces, alloy disorder, and defects, such that an atomic-level understanding becomes preferable over less computationally expensive continuum models.

The simplest and most widely used flavor of the VFF model due to Keating,[5] together with anharmonic corrections,[6] has been shown to provide reasonable agreement with experiment when it comes to the modeling of electronic states in strained nanostructures.[7] Yet, it is well known that it fails to reproduce basic bulk properties of zinc-blende crystals. It can be easily shown that the two parameters entering the Keating model provide an insufficient amount of free parameters to match the three elastic constants. Furthermore, the disregard of the partially ionic nature of the bonds in III-V materials leads to large discrepancies, especially in dynamical properties such as optical phonon modes.

Several extensions of the Keating model exist. The original valence force field model for diamond[4] was shown to possess seven independent parameters in general, three of which are related to interactions between second-nearest neighbors. These results were extended to zinc-blende structures by Martin[8] via inclusion of the Coulomb interaction between partially charged atoms within a rigid-point-ion approximation. However, the second-nearest-neighbor short-range interaction terms were neglected in Ref. 8 as well as various other works.[9–11] It was shown earlier for diamond[12] that especially the interaction associated with three connected coplanar bonds plays a significant role. In Ref. 13, the experimentally observed flattening of the TA mode near the zone boundary was explained in terms of the coplanar interaction. The importance of this interaction was advocated further in Ref. 14. Zunger *et al*. have included the stretch-bend interaction[15,16] and, on one occasion,[9] also the cross-stretch interaction in successful descriptions of GaP quantum dots,[9] InAs quantum dots,[15] InGaAs alloys,[16] and InAs/GaAs superlattices.[16]

It is known that the quasiharmonic VFF approach fails to provide even qualitative agreement with properties associated with volume expansion of the crystal.[6,13] This deficiency can be lifted by an inclusion of anharmonic corrections to the force constants. The additional parameters enable a fitting of the Grüneisen mode parameters,[17] which describe the crystal behavior under hydrostatic strain.

This work aims to unify the VFF descriptions for zinc-blende crystals by including all nearest-neighbor as well as the coplanar second-nearest-neighbor interactions, incorporating the Coulomb interaction within the rigid-ion approximation[8] and anharmonicity corrections. An in-depth analysis of the resulting VFF model is presented in an attempt to increase its applicability in zinc-blende structures.

Two central results are derived within the scope of this paper: (1) an analytic relation between the model's parameters and the second-order elastic constants, and (2) the application of the enhanced model to GaAs. The resulting model will be shown to provide a unified description of isothermal static and dynamic lattice properties of a zinc-blende crystal using a VFF approach. It agrees with reported experimental values to a satisfying degree.

After a detailed description of the model in Sec. II, analytical expressions for the elastic constants and the internal strain parameter as a function of the force constants are derived in Sec. III. These expressions extend the work in Refs. 13 and 18 by including the Coulomb interaction. In Sec. IV, parameter sets for gallium arsenide are presented, which yield good agreement between computed quantities and experimental measurements for phonon spectra, elastic constants, sound velocities, and Grüneisen coefficients. A few aspects of the model are revisited and a remark on its predictiveness is made. The paper concludes in Sec. V.

II. MODEL

This section presents the expression for the lattice energy, which constitutes the core of the model, and outlines how a number of lattice properties are obtained from it. The potential energy of the lattice is expressed in terms of atomic locations as follows:[4,13,14]

$$U = \frac{3}{16}\sum_{i,j\in NN(i)}\left[\alpha_{ij}(\delta r_{ij})^2 + \sum_{k\in NN(i)}^{k\neq j}\left(\beta_{jik}(\delta\theta_{jik})^2 + \gamma_{jik}\delta r_{ij}\,\delta\theta_{jik} + \delta_{jik}\delta r_{ij}\,\delta r_{ik} + \sum_{l\in NN(k)}^{\mathrm{COP}(j-i-k-l)}\nu_{jikl}(\delta\theta_{jik})(\delta\theta_{ikl})\right)\right] + \frac{1}{8\pi\epsilon_0}\sum_{i,j\neq i}\frac{Z_i Z_j}{|\mathbf{r}_i-\mathbf{r}_j|}, \tag{1}$$

with

$$\delta r_{ij} \equiv \frac{\left(r_{ij}^2 - d_{ij}^2\right)}{d_{ij}}, \tag{2a}$$

$$\delta\theta_{jik} \equiv \frac{(\mathbf{r}_{ij}\cdot\mathbf{r}_{ik} - \cos\theta_0 d_{ij} d_{ik})}{\sqrt{d_{ij}d_{ik}}}. \tag{2b}$$

Here, $\mathbf{r}_{ij}\equiv\mathbf{r}_j-\mathbf{r}_i$ is the bond vector pointing from atom i to atom j, d_{ij} is a model parameter, which in the absence of Coulomb interaction, represents the equilibrium length r_0 of the bond $i-j$ (see Sec. III A), θ_0 is the ideal tetrahedral bond angle, $\alpha,\beta,\gamma,\delta,\nu$ are the force constants for bond stretching, bond bending, stretch-bend interactions, cross-stretch interactions, and coplanar bend-bend interactions, respectively, and Z_i is an effective point charge sitting at atom i. The summation of i extends over all explicitly considered atoms (two for a bulk primitive zinc-blende unit cell). $NN(i)$ denotes all nearest neighbors of atom i and $\mathrm{COP}(j-i-k-l)$ denotes the condition that the bonds $j-i$, $i-k$, and $k-l$ need to be coplanar.

Any background dielectric screening of the Coulomb interaction is incorporated into the effective charges Z_i, which correspond to the Born transverse charge $e_T^* e$ in Ref. 19 with $\epsilon_\infty = 1$. For bulk zinc-blende crystals, they can be determined from the experimental longitudinal-optical–transverse-optical (LO–TO) phonon splitting at Γ using the relationship[20]

$$Z^2 = V_{\mathrm{prim}} M_r \epsilon_0\left(\omega_{\mathrm{LO}}^2 - \omega_{\mathrm{TO}}^2\right). \tag{3}$$

Here, $V_{\mathrm{prim}} = \frac{a^3}{4}$ is the volume of the primitive unit cell and $M_r \equiv \frac{M_C M_A}{M_C+M_A}$ is the reduced cation-anion mass. Thus, there is a charge $+Z$ sitting at cation sites and an opposite charge $-Z$ sitting at anion sites, as opposed to bond-charge models[2,21,22] where additional point charges are fixed at[21] or adiabatically moving around[2,22] the middle of bonds. In bulk crystals, the Coulomb interaction is computed using Ewald summation[23,24] (see Appendix A).

For zinc-blende structures, the force constants β, γ, and δ may differ depending on whether an anion (A) or a cation (C) sits at the apex of the bond angle. However, it will be shown that the lattice energy of bulk systems depends only on the arithmetic average of the two values. It is therefore convenient to define

$$\beta \equiv \frac{\beta_{ACA}+\beta_{CAC}}{2}, \tag{4}$$

and similarly for γ and δ.

Comparison to other models: The present model is similar to the one of Kane[14] but includes stretch-bend and third-order-stretching nearest-neighbor terms instead of a second-nearest-neighbor stretch term. Also, the parameter sets in Refs. 13 and 14 were exclusively fitted against selected phonon frequencies, whereas this work includes the elastic constants and the sound velocities in the fitting procedure. Finally, anharmonic parameter corrections are introduced here to obtain agreement with experimental Grüneisen parameters.

The Coulomb interaction is treated under the assumption that, as the ions oscillate, a constant fractional amount of pointlike charges moves along rigidly, generating merely a monopole field.[25] Kane's model[14] is more refined in that it incorporates a multipole-expanded Coulomb interaction. The deformation-dipole-model (DDM) of Kunc *et al.*[26] allows for an additional deformation of the electronic charge with the lattice vibration and an electronic polarizability due to microscopic fields. It was shown in Ref. 27 that an 11-parameter rigid-ion model, which is obtained from the 15-parameter DDM by neglecting polarizabilities, can match the accuracy of the DDM along high-symmetry lines of the Brillouin zone, but the two models differ in the phonon density of states, which is a signature of the entire phonon dispersion. This work assumes the rigid-ion approximation to be sufficient, and no attempts were made to fit the phonon density of states.

A. Anharmonic modifications of the force constants

The force constants are assumed to have a parametric dependence on the atomic positions[13]

$$\alpha = \alpha_0\left(1 + A_\alpha \Delta_r^{ij}\right), \tag{5a}$$

$$\beta = \beta_0\left(1 + A_\beta \Delta_r^{jik}\right), \tag{5b}$$

$$\gamma = \gamma_0\left(1 + A_\gamma \Delta_r^{jik}\right), \tag{5c}$$

$$\delta = \delta_0\left(1 + A_\delta \Delta_r^{jik}\right), \tag{5d}$$

$$\nu = \nu_0\left(1 + A_\nu \frac{\Delta_r^{jik} + \Delta_r^{ikl}}{2}\right). \tag{5e}$$

Here, the definitions

$$\Delta_r^{ij} \equiv \frac{r_{ij}^2 - r_{0,ij}^2}{2r_{0,ij}^2}, \tag{6a}$$

$$\Delta_r^{jik} \equiv \frac{r_{ij}r_{ik} - r_{0,ij}r_{0,ik}}{2r_{0,ij}r_{0,ik}} \tag{6b}$$

were made.

The dependencies in Eq. (5) are parametric in the sense that no spatial derivatives are taken during the computation of the dynamical matrix [see Eq. (9)]. The anharmonic corrections thus influence the mode Grüneisen parameters and third-order elastic constants but not the second-order elastic constants or unstrained phonon dispersions, for the terms involving Δ_r in Eq. (5) vanish in these cases.

Comparison to other models: The functional dependence in Eq. (5) is a simplified version of Sui *et al.*,[13] but differs from Refs. 6 and 28 and also from the modified VFF model in Ref. 29. In Refs. 6 and 13, additional anharmonic parameters related to bond angles are taken into account, which were derived from the shear deformation parameter. However, the authors of Ref. 30, the original source of this type of correction, argue that when using a generalized model such as the present one, such additional corrections are small. We also refrain from a further proliferation of parameters by introducing atom-type-dependent anharmonicity parameters.

Lastly, it is noted that some angle dependence is indeed included in all but the first terms of Eq. (1), and it will be shown that five independent parameters that are exclusively related to anharmonicity provide sufficient degrees of freedom to fit the corresponding Grüneisen parameters.

B. Phonon spectra

Using the ansatz

$$\mathbf{u}_{n\mathbf{q}}(i)(t) = \mathbf{u}_{n\mathbf{q}}(i)e^{i[\mathbf{q}\cdot\mathbf{r}_i-\omega_n(\mathbf{q})t]} \tag{7}$$

for an oscillating displacement $\mathbf{u}_{n\mathbf{q}}(i)(t)$ with amplitude $\mathbf{u}_{n\mathbf{q}}(i) = (u^x_{n\mathbf{q},i}, u^y_{n\mathbf{q},i}, u^z_{n\mathbf{q},i})^T$ at an atomic site i, the Newton equation of motion for the atoms becomes the eigenvalue equation[20]

$$\mathbf{D}(\mathbf{q})\mathbf{u}_{n\mathbf{q}} = \omega_n^2(\mathbf{q})\mathbf{u}_{n\mathbf{q}}, \tag{8}$$

where $\omega_n(\mathbf{q})$ is the phonon frequency of branch n and wave vector $\mathbf{q}$. The dynamical matrix $\mathbf{D}$ is related to the second derivatives of the potential energy by[9,23]

$$D_{i\mu,j\nu}(\mathbf{q}) = \frac{1}{\sqrt{M_i M_j}} \sum_l \frac{\partial^2 U}{\partial r_i^\mu \partial \left(r_j^\nu + R_l^\nu\right)} e^{-i\mathbf{q}\cdot\mathbf{R}_l}. \tag{9}$$

Here, i and j denote atomic indices in the primary unit cell, M_i and M_j are the respective masses, $\mu,\nu \in \{x,y,z\}$, and l runs over all lattice vectors $\mathbf{R}_l$.

C. Elastic constants and internal strain parameter

In the presence of homogeneous strain, the Bravais vectors $\mathbf{a}_i$ of the crystal experience a distortion

$$\mathbf{a}_i' = (\mathbf{1}+\boldsymbol{\epsilon})\mathbf{a}_i, \tag{10}$$

where $\boldsymbol{\epsilon}$ is the (infinitesimal) strain tensor. In addition, the two-atom zinc-blende primitive unit cell composed of a cation at $\mathbf{r}_C = 0$ and an anion at $\mathbf{r}_A = \frac{a}{4}(1,1,1)$ can be distorted internally by an additional displacement of one atom with respect to the other:[13,20]

$$\mathbf{r}_A' = (\mathbf{1}+\boldsymbol{\epsilon})\mathbf{r}_A - \xi\frac{a}{2}\begin{pmatrix}\epsilon_{yz}\\ \epsilon_{xz}\\ \epsilon_{xy}\end{pmatrix}. \tag{11}$$

Here, ξ denotes Kleinman's internal strain parameter. A relationship between ξ and the force constants can be found by a condition of minimal energy[13]

$$\left.\frac{\partial U}{\partial \xi}\right|_{\xi=\xi_0} = 0. \tag{12}$$

D. Sound velocities and Grüneisen mode parameters

The sound velocities of acoustic branches

$$c_s^n \equiv \frac{\partial\omega_n(0)}{\partial q} \tag{13}$$

and the Grüneisen mode parameters[17]

$$\gamma_n(\mathbf{q}) \equiv \frac{V_{\text{prim}}}{\omega_n(\mathbf{q})}\frac{\partial\omega_n(\mathbf{q})}{\partial V_{\text{prim}}} \tag{14}$$

can be determined numerically from the computed phonon spectra (see also comment in Appendix A). The authors observed that the small-strain limit for the Grüneisen parameters is only reached for bond length distortions below 0.01%. However, the results in Sec. IV are computed using a hydrostatic strain of 0.03, corresponding to a bond elongation of 1%. This yields values for the Grüneisen coefficients, which can differ by as much as 10% from the converged small-strain values. This choice was made in anticipation of nonvanishing strain in nanostructures. It is also noted that $\gamma_{\text{LO}}(\Gamma)$ and $\gamma_{\text{TO}}(\Gamma)$ have the same value in the limit of vanishingly small strain, but the reported experimental values (see Table II) exhibit a split.

III. ANALYTICAL RESULTS

This section presents analytical results following from the model in Sec. II. First, it is shown that the model parameter d can not simply be chosen as the equilibrium bond length in a polar crystal if the consistency of the model is to be preserved. Second, material properties such as the elastic constants are expressed in terms of the model input parameters.

A. Coulomb-induced modification of the model parameter *d*

Using Eqs. (1)–(6), the crystal energy of a bulk zinc-blende primitive unit cell in equilibrium can be found by inserting the atomic positions and exploiting periodicity. It evaluates to

$$U_{\text{bulk}}^{\text{unstrained}} = \left(F + G\frac{r_0^2-d^2}{2d^2}\right)\frac{\left(r_0^2-d^2\right)^2}{2d^2} + \alpha_M\frac{S}{r_0}, \tag{15}$$

where

$$S \equiv \frac{Z^2}{4\pi\epsilon_0} \tag{16}$$

is the strength of the Coulomb interaction, r_0 is the bond length, and the definitions

$$F \equiv 3\alpha_0 + \beta_0 - 3\gamma_0 + 9\delta_0 + \nu_0, \tag{17a}$$

$$G \equiv 6\alpha_0 r_0 A_\alpha + \beta_0 A_\beta - 3\gamma_0 A_\gamma + 9\delta_0 A_\delta + \nu_0 A_\nu \tag{17b}$$

were made. α_M is the Madelung constant for zinc-blende

$$\alpha_M \equiv -1.638\,055\,053\,388\,790. \tag{18}$$

The constant was computed to this accuracy by equating $\alpha_M\frac{S}{r_0}$ with the numerically evaluated Ewald sum (see Appendix A).

As pointed out in Ref. 31, the energy of an unstrained bulk crystal should be minimal at the experimental bond length $r_{0,\text{exp}}$ in order for the model to be consistent. The attractive Coulomb energy shifts the minimum to smaller bond lengths

and, hence, d must be modified to counterbalance this effect. Applying the condition

$$\left.\frac{\partial U_{\text{bulk}}^{\text{unstrained}}}{\partial r_0}\right|_{r_0=r_{0,\text{exp}}} = 0 \tag{19}$$

to Eq. (15) yields a relation between d and the experimental bond length. In the absence of anharmonic corrections, the relation reads as

$$d^2 = r_{0,\text{exp}}^2 \frac{1}{1+S_1}, \tag{20}$$

where

$$S_1 \equiv S\frac{\alpha_M}{2Fr_{0,\text{exp}}^3}. \tag{21}$$

When anharmonic corrections are included, the relation becomes

$$d^2 = r_{0,\text{exp}}^2 \frac{2+\frac{G}{2F}}{1+S_1+\frac{G}{2F}+\sqrt{(1+S_1)^2+\frac{G}{F}S_1}}. \tag{22}$$

The experimental bond length $r_{0,\text{exp}}$ will henceforth be called r_0. We find that the analytical expressions in the following section become intractable when using Eq. (22). Hence, Eq. (20) is used for all subsequent results, including the parameter fitting, causing a minor inconsistency of the model. Using this approach, the force constants as well as the parameter d are not influenced by the anharmonicity constants in an unstrained crystal. Thus, the unstrained phonon spectra remain unchanged with respect to the choice of the anharmonic coefficients. The influence of the choice of d is revisited in Sec. IV C.

B. Elastic constants, internal strain parameter, and sound velocities

Using the program Mathematica, Eqs. (10) and (11) can be inserted into Eq. (1) for the primitive zinc-blende unit cell, using Eq. (A1) for the Coulomb term. A Taylor expansion to second order in ϵ_{ij} can then be compared to the total energy per primitive unit cell in terms of the elastic constants[13]

$$\begin{aligned}\frac{U(\boldsymbol{\epsilon})}{V_{\text{prim}}} = \frac{U(0)}{V_{\text{prim}}} &+ \frac{C_{11}}{2}\left(\epsilon_{xx}^2+\epsilon_{yy}^2+\epsilon_{zz}^2\right)\\ &+ C_{12}(\epsilon_{xx}\epsilon_{yy}+\epsilon_{xx}\epsilon_{zz}+\epsilon_{yy}\epsilon_{zz})\\ &+ 2C_{44}\left(\epsilon_{xy}^2+\epsilon_{xz}^2+\epsilon_{yz}^2\right).\end{aligned} \tag{23}$$

The result reads as

$$C_{11} = \frac{\sqrt{3}}{4r_0}\left((\alpha_0+3\beta_0-\gamma_0+3\delta_0+3\nu_0)+(5\alpha_0+7\beta_0-5\gamma_0+15\delta_0+7\nu_0)\frac{S_1}{2}\right)+\mathcal{B}\frac{S}{r_0^4}, \tag{24a}$$

$$C_{12} = \frac{\sqrt{3}}{4r_0}(\alpha_0-\beta_0-\gamma_0+3\delta_0-\nu_0)(1+S_1)+\mathcal{C}\frac{S}{r_0^4}, \tag{24b}$$

$$\begin{aligned}C_{44} = \frac{\sqrt{3}}{4r_0}\Bigg(&[(1-\xi)^2\alpha_0+(1+\xi)^2\beta_0-(1-\xi^2)\gamma_0-(1-\xi)^2\delta_0+(1+\xi)^2\nu_0]+[7\alpha_0+5\beta_0-7\gamma_0+5\delta_0+5\nu_0\\ &+8(-\alpha_0+\beta_0+\delta_0+\nu_0)\xi+2(5\alpha_0-\beta_0+5\gamma_0+7\delta_0-\nu_0)\xi^2]\frac{S_1}{4}\Bigg)+\left(\mathcal{D}+\mathcal{E}\xi-\frac{3\pi}{64}\xi^2\right)\frac{S}{r_0^4},\end{aligned} \tag{24c}$$

$$\xi = \frac{(\alpha_0-\beta_0-\delta_0-\nu_0)(1+S_1)-\frac{2\mathcal{E}S}{\sqrt{3}r_0^3}}{(\alpha_0+\beta_0+\gamma_0-\delta_0+\nu_0)+(5\alpha_0-\beta_0+5\gamma_0+7\delta_0-\nu_0)\frac{S_1}{2}-\frac{\sqrt{3}\pi S}{16r_0^3}}. \tag{24d}$$

Here, the numerical constants $\mathcal{B}$, $\mathcal{C}$, $\mathcal{D}$, $\mathcal{E}$ are

$$\mathcal{B} \equiv +0.034\,811\,170\,691\,607, \tag{25a}$$

$$\mathcal{C} \equiv -0.194\,730\,246\,474\,826, \tag{25b}$$

$$\mathcal{D} \equiv -0.106\,067\,915\,910\,315, \tag{25c}$$

$$\mathcal{E} \equiv +0.707\,179\,791\,600\,111. \tag{25d}$$

The constants β_0, γ_0, and δ_0 in Eqs. (24a)–(24d) represent the averages between anion and cation values, as defined in Eq. (4). This averaging is not an approximation but an outcome of the calculation that is related to the symmetry properties of the crystal.

From Eqs. (15) and (24a)–(24d), it can be seen that (a) the contributions of the harmonic parameters to the crystal energy have the same order of magnitude and (b) there is an intricate interplay between the parameters when it comes to crystal distortions. It is therefore nontrivial to make any judgment on the signs that the parameters should have. Indeed, any combination of positive and negative parameters will increase the crystal energy in the presence of distortions as long as the resulting elastic constants are positive. This situation is further complicated by the fact that the elastic constants are invariant with respect to sign inversion of the cation and anion values of β, γ, and δ.

Comparison to other models and validation: It is important to put Eqs. (24a)–(24d) in context with earlier work. The equations are consistent with Ref. 13 in the limit of nonionic crystals, apart from the prefactor in front of δ_0 in the expression for C_{44}. The numerical constant $\mathcal{B}$ is very close to equivalent expressions found in Refs. 1 and 32, the results of which are used in other work related to the Coulomb interaction in zinc-blende crystals.[33,34] However, the cited calculations assume two-body central forces for the repulsive interaction, while Eq. (1) violates this assumption. Although the purely Coulombic terms are not influenced by this disparity, a deviation from the total expressions for the elastic constants

obtained in Refs. 1 and 32 can be expected. Furthermore, a comparison of the Coulomb energies for an unstrained crystal and a crystal with small hydrostatic strain yields the relation

$$\mathcal{C} = \frac{3\sqrt{3}\alpha_M}{16} - \frac{\mathcal{B}}{2}, \tag{26}$$

which is fulfilled by the values in Eqs. (25a) and (25b).

Another validation of Eqs. (24a)–(24d) is given by comparison to sound velocities evaluated from Eq. (13). The following relations hold for cubic crystals:[20]

$$c_s^{\mathrm{TA}}[100] = \sqrt{C_{44}/\rho}, \tag{27a}$$
$$c_s^{\mathrm{LA}}[100] = \sqrt{C_{11}/\rho}, \tag{27b}$$
$$c_s^{\mathrm{TA1}}[110] = \sqrt{(C_{11}-C_{12})/(2\rho)}, \tag{27c}$$
$$c_s^{\mathrm{TA2}}[110] = \sqrt{C_{44}/\rho} = c_s^{\mathrm{TA}}[100], \tag{27d}$$
$$c_s^{\mathrm{LA}}[110] = \sqrt{(C_{11}+2C_{12}+4C_{44})/(2\rho)}, \tag{27e}$$
$$c_s^{\mathrm{TA}}[111] = \sqrt{(C_{11}-C_{12}+C_{44})/(3\rho)}, \tag{27f}$$
$$c_s^{\mathrm{LA}}[111] = \sqrt{(C_{11}+2C_{12}+4C_{44})/(3\rho)}, \tag{27g}$$

where $\rho = 4(M_C + M_A)/a^3$ is the mass density. These simple relations are indeed satisfied by the results in Sec. IV. Using Eqs. (24) and (27), the elastic constants and sound velocities can be predicted analytically from the VFF parameters without the need for numerical phonon energy computations.

IV. RESULTS FOR GALLIUM ARSENIDE

This section presents and discusses sets of force constants obtained by numerically fitting the model outcomes against experimental targets. It is anticipated that the importance of the different lattice properties varies with the application of the model, and that parameters can be specialized to model certain problems particularly well. For example, in thermal transport problems, the elastic constants may be disregarded for the benefit of having a better fitted phonon dispersion. On the other hand, the influence of optical modes is expected to be negligible in lattice relaxation problems or low-gradient phonon transport. Neglecting the Coulomb interaction, which poses tremendous computational challenges in large systems, is thus desirable for such problems. Six different parameter sets are therefore presented in this paper:

(1) The full-fledged model presented in the preceding sections, termed P8, consists of eight parameters for unstrained zinc-blende materials and an additional five parameters related to anharmonicity corrections. The parameters were fitted against targets for the phonon dispersion along three symmetry lines, sound velocities, elastic constants, and (for the anharmonicity corrections) Grüneisen parameters.

(2) A simpler fit termed P5 assumes the parameters β, γ, and δ to be the same for anions and cations, resulting in five free parameters for the unstrained case.

(3,4) Two fits against the acoustic phonon branches and elastic constants were performed under exclusion of the Coulomb interaction (P8/C, P5/C).

(5,6) Fits were performed against all phonon branches, disregarding the elastic constants (P8/el, P5/el).

The results of several other fits are not reported in detail here. It was empirically found that fits of the acoustic branches alone do not yield any significant improvement over the P8/C and P5/C fits. Fits of the acoustic branches and elastic constants, which include the Coulomb interactions, also do not improve the P8/C and P5/C fits, as can be expected. The authors also tried a six-parameter model where the stretch-bend interaction was neglected. This model yielded no significant improvement over the five-parameter model.

As already mentioned in Sec. III B, an *a priori* determination of the correct signs of the model parameters β, γ, and δ is not straightforward. The authors' experience is that fits of similar quality can be achieved with combinations of different, sometimes opposite, signs, thus suggesting ambiguities in the model parameters. For the lack of better knowledge, the convention is made that the cation values of γ and ν be positive and the anion values be negative in the P8/el and P8/C fits. Furthermore, all parameters are chosen to be non-negative in the P5 fits. The numerical computation of all quantities was performed using NEMO5, a nanoelectronics modeling tool developed by the authors to obtain a diverse range of nanostructure characteristics. The details of NEMO5 are presented elsewhere.[35] The implementation was validated against literature results.[6,11,13,18,36]

A. Model parameter sets and comparison to experimental values

The fitted parameter sets are displayed in Table I. The procedure for obtaining these sets via genetic algorithms is outlined in Appendix B and, to a more detailed extent, in Ref. 37. Table II compares the model outcomes and experimental targets. Experimental values for the targets are taken from Ref. 38 for the room-temperature elastic constants C_{ij} and sound velocities c_s. The value of the internal strain parameter ξ has a large uncertainty,[39] but seems to be roughly 0.55.[40] Data from Ref. 41 are used for the phonon spectra and frequencies at high-symmetry points. It is noted that, even though the measurements in Ref. 41 were taken at $T =$ 12 K, the temperature dependence is expected to be relatively small[42] and the authors were unable to find comparable room-temperature data. Targets for the Grüneisen parameters are taken from experimental data[43] for $\gamma_{\mathrm{LO,TO}}(\Gamma)$, $\gamma_{\mathrm{TO,TA}}(X)$, and $\gamma_{\mathrm{TO,TA}}(L)$ and from *ab initio* calculations[44] for $\gamma_{\mathrm{LO,LA}}(X)$ and $\gamma_{\mathrm{TO,TA}}(L)$. The calculations use a lattice constant of $a = 0.565\,324$ nm and atomic masses $M_{\mathrm{Ga}} = 69.723$ amu and $M_{\mathrm{As}} = 74.92160$ amu.

B. Discussion of the fits

1. Best overall fit

Phonon spectra. Figure 1 shows the result obtained by fitting the eight-parameter model against the sound velocities, the elastic constants, and the entire phonon dispersion (P8 parameter set). Also plotted for comparison is the Keating model with Martin's parameters,[8] which were optimized for the elastic constants. The P8 fit slightly overestimates the coplanar interaction, as can be seen by the negative slope of the

TABLE I. Force constants [see Eq. (1)] and anharmonicity correction parameters [see Eq. (5)] for gallium arsenide. The columns correspond to the full model (P8), five-parameter model (P5), eight-parameter model excluding Coulomb interaction (P8/C), five-parameter model excluding Coulomb interaction (P5/C), eight-parameter model disregarding the elastic constants (P8/el), and five-parameter model disregarding the elastic constants (P5/el).

Constant	P8	P5	P8/C	P5/C	P8/el	P5/el
α_0 (N/m)	38.8356	39.3883	45.0000	38.9425	43.2347	43.8470
$\beta_{0,ACA}$ (N/m)	1.9074	2.8660	13.0980	4.0663	− 2.6178	3.1854
$\beta_{0,CAC}$ (N/m)	12.8298	2.8660	− 5.1908	4.0663	11.3187	3.1854
$\gamma_{0,ACA}$ (N/m)	81.6749	0.0	19.2399	0.0	48.0814	0.0
$\gamma_{0,CAC}$ (N/m)	− 88.4692	0.0	− 22.4448	0.0	− 54.3912	0.0
$\delta_{0,ACA}$ (N/m)	45.6625	1.7962	5.1675	0.0	22.0988	4.5357
$\delta_{0,CAC}$ (N/m)	− 43.7240	1.7962	− 10.0261	0.0	− 16.4250	4.5357
ν_0 (N/m)	1.9238	6.5832	5.6298	5.8559	3.3087	3.9710
Z (e)	0.658741	0.658741	0.0	0.0	0.658741	0.658741
A_α (nm^{-1})	− 13.1091	− 12.1307	− 11.5785	− 12.9325	− 13.0084	− 12.1712
A_β	− 2.7353	− 11.3577	− 4.8975	− 3.5689	− 10.3376	− 15.0271
A_γ	− 3.2391		− 15.4117		− 11.3817	
A_δ	− 10.0070	1.1664	− 11.0843		− 7.2233	− 3.0958
A_ν	− 23.1807	− 5.8621	− 5.4246	− 3.7367	6.6924	− 4.6313

TA branch around X, and has a large imbalance between anion and cation parameters. Also, the main quantitative deviations to experimental data occur at the zone boundary between X and K, where the rigid-ion model is most likely to break down.[27]

Grüneisen parameters. As mentioned in Sec. II A, the Grüneisen parameter fits in Table II were obtained by comparing the phonon frequencies for a hydrostatic strain of 0.03 with the unstrained phonon frequencies. This may yield results that differ from the small-strain limit by as much as 10%. An accurate modeling of Grüneisen parameters has been problematic in the past. *Ab initio* calculations exhibit deviations from experiment of up to a factor of 2.[3,45] Reference 17 used a rigid-ion model to obtain results within 20% of experiment. In Ref. 46, a bond-charge model calculation yielded agreement on the order of 10% or better when employing a finite hydrostatic strain of 0.01 for the finite-difference extraction. In Ref. 6, a different type of anharmonic correction was used to obtain the correct signs of all but one of the Grüneisen parameters within a Keating VFF description; however, differences to experimental values of up to 90% remained. With these prior efforts in mind, and given some uncertainty about experimental methods, the maximum discrepancy of 22% in the fits of the Grüneisen parameters of the P8 model can be termed sufficiently accurate.

2. *Five-parameter fit*

The five-parameter fit is in qualitative disagreement with experiment for the optical branches along the Σ line and overestimates the maximum of the upper transverse acoustic (TA) mode around K. An accurate model for these parts of the phonon dispersion should employ eight parameters. However, the five-parameter model offers a good description of the low-frequency acoustic branches as well as the elastic constants (see Fig. 2). The maximum deviation from experiment for the lower TA mode occurs at L (12%). The Grüneisen parameters are fit better than for the P8 set, with a maximum discrepancy of 14%.

From Table I, it is observed that the best five-parameter fits employ no stretch bend and only a small, if any, cross-stretch interaction. This stands in contrast to the coplanar interaction, which is essential in order to obtain flattened TA branches around X and L. Neglecting the coplanar interaction term results in either an overestimation of the zone-boundary phonon frequencies[8] or an underestimation of the frequencies around the zone center and the speed of sound (such as with the $n=1$ parameters in Ref. 14). In Ref. 14, the cross-stretch interaction was termed the least important out of all considered ones (the stretch-bend term was not included), which is consistent with the present findings. It was found in the scope of this work, however, that a six-parameter model, which takes into account the different atom types but neglects the stretch-bend term, does not yield fits of the same quality as the eight-parameter model.

3. *Fits neglecting the elastic constants*

The requirement of matching the elastic constants is relaxed in the fits displayed in Fig. 3. The fitting process still incorporates the sound velocities to a small extent in order to retain physically meaningful values. The P8/el fit of the phonon dispersion seems less forced than the P8 fit and has parameters of smaller magnitude, but it allows for discrepancies versus experimental values of up to 40% in the elastic constants (see Table II). The discrepancy of the upper TA mode around K is larger than in the P8 set, suggesting that atom-type-dependent parameters, which are large and of roughly opposite magnitude, are required to fit it. The P5/el set models most of the phonon dispersion to a satisfactory degree, but has both qualitative and quantitative deficiencies along the Σ line near the zone boundary. The Grüneisen parameters are generally modeled well, with the exception of $\gamma_{\mathrm{LA}}(L)$ in the P8/el set. As with the P8 and P5 fits, the P5/el fit of the Grüneisen parameters has less deviations (maximum 11%) than the P8/el fit (maximum 32%).

TABLE II. Comparison of literature values versus model results for the lattice properties of GaAs. The different models P8, P5, P8/C, P5/C, P8/el, and P5/el are discussed in the text. The column to the right of P8 displays the deviation (Dev.) between calculated and experimental (Expt.) values.

Quantity (unit)	Expt.	P8	Dev.	P5	Dev.	P8/C	Dev.	P5/C	Dev.	P8/el	Dev.	P5/el	Dev.
C_{11} (GPa)	119.0	120.20	1%	120.35	1%	120.83	2%	121.54	2%	129.32	9%	131.29	10%
C_{12}	53.4	55.53	4%	54.63	2%	51.33	−4%	51.33	−4%	75.43	41%	80.77	51%
C_{44}	59.6	58.26	−2%	54.57	−8%	58.86	−1%	55.95	−6%	51.42	−14%	45.52	−24%
$c_s^{\mathrm{TA}}[100]$ (km/s)	3.34	3.31	−1%	3.20	−4%	3.32	−1%	3.24	−3%	3.11	−7%	2.93	−12%
$c_s^{\mathrm{LA}}[100]$	4.73	4.75	0%	4.76	1%	4.76	1%	4.78	1%	4.93	4%	4.97	5%
$c_s^{\mathrm{TA1}}[110]$	2.47	2.47	0%	2.49	1%	2.55	3%	2.57	4%	2.25	−9%	2.18	−12%
$c_s^{\mathrm{TA2}}[110]$	3.34	3.31	−1%	3.20	−4%	3.33	0%	3.24	−3%	3.11	−7%	2.93	−12%
$c_s^{\mathrm{LA}}[110]$	5.24	5.24	0%	5.17	−1%	5.22	0%	5.17	−1%	5.38	3%	5.34	2%
$c_s^{\mathrm{TA}}[111]$	2.78	2.78	0%	2.75	−1%	2.83	2%	2.81	1%	2.57	−8%	2.45	−12%
$c_s^{\mathrm{LA}}[111]$	5.39	5.40	0%	5.30	−2%	5.36	−1%	5.30	−2%	5.52	2%	5.46	1%
ξ	ca.0.55	0.575	5%	0.526	−4%	0.67	22%	0.59	7%	0.67	22%	0.634	15%
$\hbar\omega_{\mathrm{LO}}(\Gamma)$ (meV)	36.35	36.07	−1%	37.16	2%	40.23	11%	37.58	3%	36.50	0%	36.98	2%
$\hbar\omega_{\mathrm{TO}}(\Gamma)$	33.62	33.17	−1%	34.35	2%	40.23	20%	37.58	12%	33.63	0%	34.15	2%
$\hbar\omega_{\mathrm{LO}}(X)$	29.78	28.90	−3%	27.73	−7%	29.27	−2%	28.15	−5%	29.30	−2%	29.14	−2%
$\hbar\omega_{\mathrm{TO}}(X)$	31.80	32.42	2%	30.11	−5%	37.09	17%	33.55	6%	32.12	1%	31.00	−3%
$\hbar\omega_{\mathrm{LA}}(X)$	27.91	27.20	−3%	26.76	−4%	27.76	−1%	27.15	−3%	27.57	−1%	28.11	1%
$\hbar\omega_{\mathrm{TA}}(X)$	10.13	8.93	−12%	10.58	4%	10.06	−1%	10.83	7%	10.00	−1%	10.93	8%
$\hbar\omega_{\mathrm{LO}}(L)$	29.98	30.45	2%	27.61	−8%	31.67	6%	29.34	−2%	30.97	3%	29.37	−2%
$\hbar\omega_{\mathrm{TO}}(L)$	32.67	32.04	−2%	32.28	−1%	38.64	18%	35.62	9%	32.62	0%	32.60	0%
$\hbar\omega_{\mathrm{LA}}(L)$	25.64	24.81	−3%	25.21	−2%	23.47	−8%	23.56	−8%	24.64	−4%	26.14	2%
$\hbar\omega_{\mathrm{TA}}(L)$	7.86	8.83	12%	6.92	−12%	7.35	−6%	7.66	−3%	7.59	−3%	7.22	−8%
$\gamma_{\mathrm{LO}}(\Gamma)$	1.23	1.34	9%	1.23	0%	1.23	0%	1.31	7%	1.16	−6%	1.23	0%
$\gamma_{\mathrm{TO}}(\Gamma)$	1.39	1.50	8%	1.36	−2%	1.23	−12%	1.31	−6%	1.28	−8%	1.36	−2%
$\gamma_{\mathrm{LO}}(X)$	1.01	0.79	−22%	1.11	10%	1.21	20%	1.16	15%	1.19	18%	1.12	11%
$\gamma_{\mathrm{TO}}(X)$	1.73	1.51	−13%	1.73	0%	1.49	−14%	1.69	−2%	1.73	0%	1.74	1%
$\gamma_{\mathrm{LA}}(X)$	1.22	1.44	18%	1.11	−9%	1.01	−17%	1.16	−5%	1.08	11%	1.12	−8%
$\gamma_{\mathrm{TA}}(X)$	−1.62	−1.86	15%	−1.39	−14%	−1.75	8%	−1.57	−3%	−1.62	0%	−1.44	−11%
$\gamma_{\mathrm{LO}}(L)$	1.62	1.38	−15%	1.59	−2%	1.52	−6%	1.71	6%	1.53	−6%	1.60	−1%
$\gamma_{\mathrm{TO}}(L)$	1.5	1.59	6%	1.51	1%	1.34	−11%	1.47	−2%	1.51	1%	1.52	1%
$\gamma_{\mathrm{LA}}(L)$	0.56	0.68	21%	0.64	14%	0.57	2%	0.55	−2%	0.74	32%	0.60	7%
$\gamma_{\mathrm{TA}}(L)$	−1.7	−1.45	−15%	−1.92	13%	−1.75	3%	−1.76	4%	−1.70	0%	−1.87	10%

4. Fits neglecting Coulomb interaction

For the modeling of large nanostructures consisting of thousands or millions of atoms, the long-range Coulomb interaction poses a serious challenge as it destroys the sparsity of the involved matrices. The P8/C and P5/C parameter sets were obtained by fitting the acoustic phonon branches as well as the elastic constants without Coulomb interaction. The obtained fits (Fig. 4) are sufficiently good as long as the optical modes are not of critical interest. The dispersion curves are lacking any LO–TO splitting and overestimate the optical phonon energies in general. Main deviations in the acoustic branches occur for the upper TA branch near K and the longitudinal acoustic (LA) branch near L. The Grüneisen parameters for the acoustic modes are generally modeled well.

C. Discussion of some model aspects

1. Influence of the correction of d

In Sec. III A, it was argued that the model parameter d must deviate from the experimental bond length r_0 in the presence of Coulomb interaction. Figure 5 displays the phonon dispersion obtained with the P8 parameter set for three different choices of d: d according to Eq. (20) (same as Fig. 1), $d=r_0$, and d according to Eq. (22). It is apparent that the choice of d has a large influence on the obtained results, and the parameter sets need to be consistent with this choice. d typically differs from r_0 by 1.5%–2%, but the simplification of using Eq. (20) instead of (22) only imposes minor changes on the order of $10^{-4}r_0$ on the bond length and 0.1 meV (<1%) on the dispersion. This provides an *a posteriori* justification of the simplification of using Eq. (20) instead of (22). The three cases reduce to one in the absence of Coulomb interaction.

2. Anharmonicity and the elastic constants

Equations (24) for the second-order elastic constants is exact as long as the functional dependence of the VFF parameters on the bond lengths, given in Eq. (5), is taken to be parametric, i.e., no spatial derivatives of the force constants are taken for the energy gradient and the dynamical matrix. Table III illustrates the difference to the case when the derivatives are included. A difference of up to 28% is

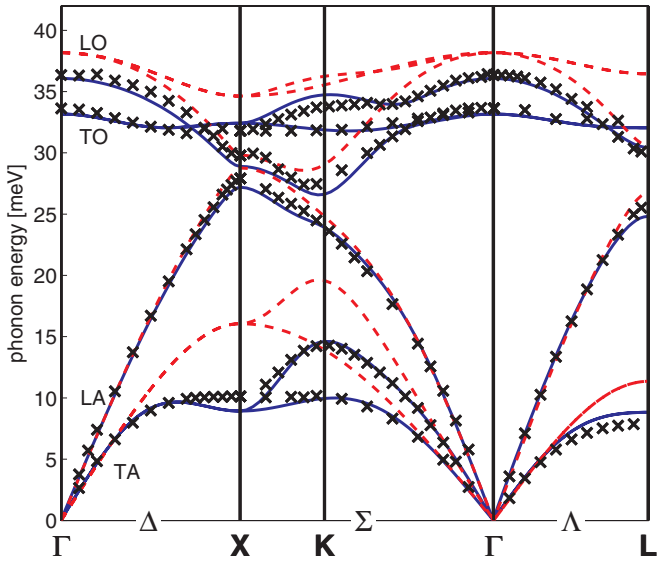

FIG. 1. (Color online) Phonon dispersion of gallium arsenide. Solid line: P8 set of parameters (see Table I) fitted against the dispersion, the sound velocities, and the elastic constants. Dashed line: Keating model with $\alpha = 41.19\frac{N}{m}$, $\beta = 8.94\frac{N}{m}$[8]. Crosses: Experimental data (Ref. 41).

observed when including Coulomb interactions, compared to less than 3% difference without it. The Coulomb interaction introduces a monotonically decaying long-range potential, which is counterbalanced with the short-range VFF potential such that an energetic minimum energy at the equilibrium bond length is achieved. However, the short-range potential taken by itself has a nonvanishing first derivative $\frac{\partial \delta r_{ij}}{\partial \epsilon}$ at this position, and anharmonicity thus yields contributions of the form $\frac{\partial \alpha}{\partial \epsilon}\frac{\partial \delta r_{ij}}{\partial \epsilon}$. The parametric dependence assumption therefore has a strong influence on the second-order elastic constants in systems with Coulomb interaction.

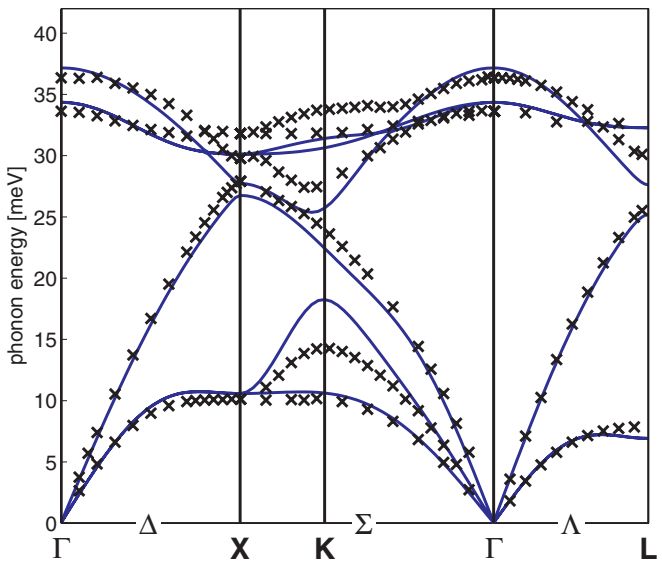

FIG. 2. (Color online) Phonon dispersion of gallium arsenide obtained with the five-parameter model (see Table I). Solid line: P5 parameter set. Crosses: Experimental data (Ref. 41).

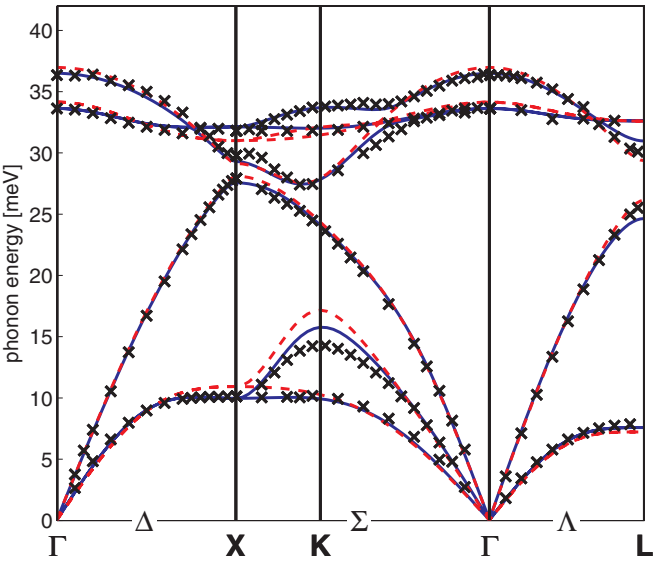

FIG. 3. (Color online) Comparisons of results obtained using models fitted exclusively against the dispersion relation (see Table I). Solid line: P8/el parameter set. Dashed line: P5/el parameter set. Crosses: Experimental data (Ref. 41).

The authors have also derived equations for the six independent third-order elastic constants[47,48] under the assumption of a full (not parametric) anharmonic dependence of the VFF parameters. This can be achieved by expanding Eqs. (1) and (5) up to third order in the infinitesimal strain ϵ_{ij} and transforming the results to the expansion in terms of the Lagrangian strain.[47,48] The third-order expansion of the energy depends heavily on the parametric dependence assumption. Alternatively, third-order constants can be extracted numerically from the dependence of the sound velocities

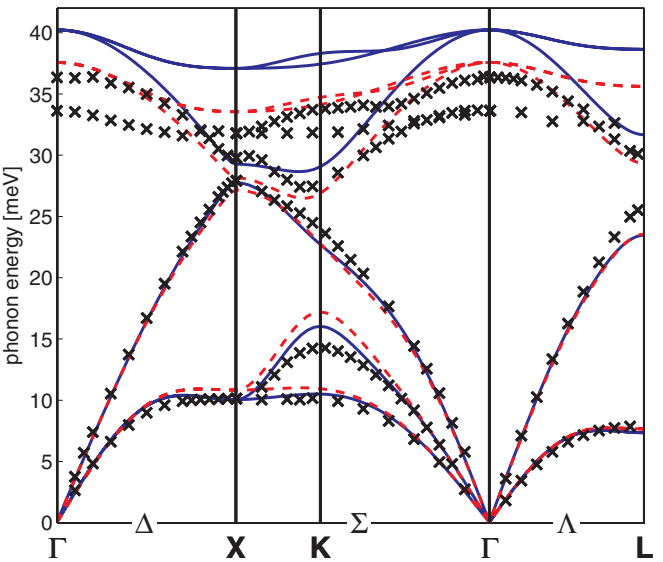

FIG. 4. (Color online) Comparisons of results obtained using models without Coulomb interaction (see Table I). The parameter sets were obtained by fitting the acoustic branches and sound velocities, as well as the elastic constants. Solid line: P8/C parameter set. Dashed line: P5/C parameter set. Crosses: Experimental data (Ref. 41).

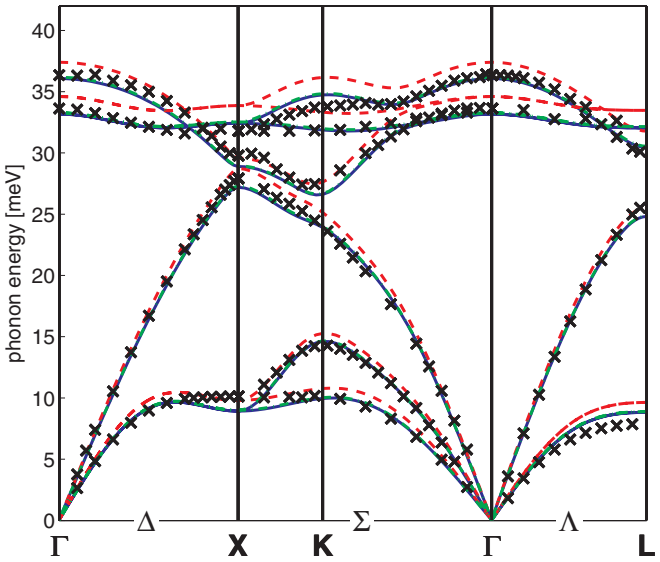

FIG. 5. (Color online) Phonon dispersion of GaAs using the P8 parameter set in Table I and different choices of d. Solid line: d according to Eq. (20). This was the choice for the fit. Dashed line: $d = r_0$. Dashed-dotted line: (almost overlapping with the solid curve) Eq. (22). Crosses: Experimental data (Ref. 41).

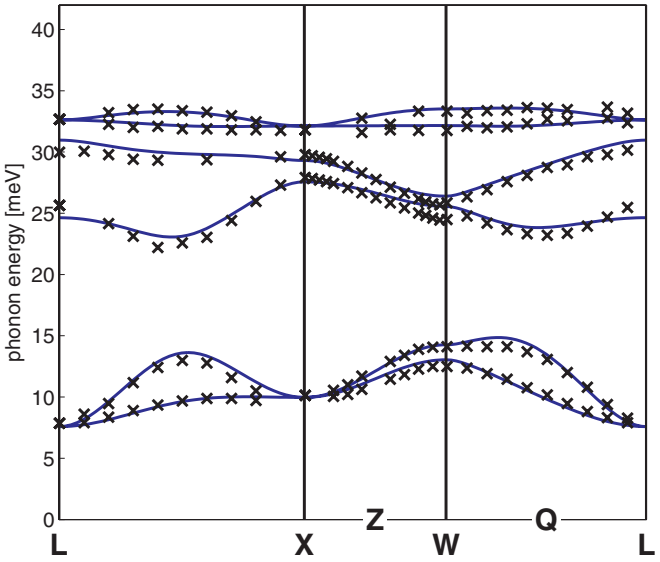

FIG. 6. (Color online) Phonon dispersion of GaAs along the path $L - X - W - L$. Solid line: P8/el parameter set (see Table I). Crosses: Experimental data (Ref. 41).

on hydrostatic and uniaxial pressure.[49] Incorporation of the third-order constants into the fitting process and understanding the relationship between third-order constants and anharmonic VFF parameters is the scope of future work.

3. *Predictiveness of the model*

The strength of any model is given by its ability to predict experimental data not included in the fitting process. While applications to nanostructures lie outside the scope of this work, a first indication of the model's predictive abilities is given by phonon frequencies, which were not included in the fitting process. Figure 6 compares the model versus experiment for the phonon dispersion path $L - X - W - L$. Good agreement is observed, suggesting a solid physical foundation of the chosen approach.

TABLE III. Influence of the anharmonicity model on the second-order elastic constants. Here, param. denotes the values for a model where the dependence of the VFF parameters on the bond stretching [Eqs. (5)] is taken to be parametric, i.e., no spatial derivatives are included in the dynamical matrix. The second-order elastic constants are then independent of the anharmonicity parameters [Eqs. (24)]. Here, full denotes the values for a model where such derivatives are included.

Parameter set	P8	P5	P8/C	P5/C
C_{11} (param.) (GPa)	120.2	120.4	120.8	121.5
C_{11} (full) (GPa)	140.5	137.0	120.4	121.5
C_{12} (param.) (GPa)	55.53	54.63	51.33	51.33
C_{12} (full) (GPa)	75.70	71.20	52.59	51.33
C_{44} (param.) (GPa)	58.26	54.57	58.86	55.95
C_{44} (full) (GPa)	61.73	58.43	57.95	55.95

V. CONCLUSION

This paper presents an extended valence force field model for the static and dynamic lattice properties of zinc-blende crystals, and applies it to gallium arsenide. The goal of the model is to provide a unified VFF description of isothermal elastic properties as well as phonon modes that agree with experiment. Computational methods, in particular, the software Mathematica for analytical transformations and NEMO5 (Ref. 35) for numerical phonon-dispersion calculations, enable the following two main results: Eqs. (24), an expression for the elastic constants in zinc-blende materials as a function of the force constants and the fractional ionic charges, and Table I, parameter sets for gallium arsenide that are found by fitting against published experimental values. Good agreement between model and experiment was achieved for all considered quantities, surpassing prior VFF-based efforts.

The P8 parameter set represents the most consistent fit, but it is shown that for practical purposes good results can also be achieved using less parameters. The P5/C set, which excludes Coulomb interaction, may be employed for the static strain relaxation in nanostructures. The P5/el and P8/el models may be useful in the modeling of thermal transport or electron-phonon interactions.

ACKNOWLEDGMENTS

The authors would like to thank R. Martin and Y.-M. Niquet for discussions as well as J. Geng, Y. He, K. Miao, and P. Sengupta for their help. This work was partially supported by Grant No. EEC-0228390 of the National Science Foundation (NSF) that funds the Network for Computational Nanotechnology and by NSF PetaApps Grant No. OCI-0749140. Support by the Semiconductor Research Corporation (SRC) and Intel Corporation is acknowledged.

APPENDIX A: EWALD SUM

An accurate computation of the long-range Coulomb interaction energy in a bulk crystal with point charges Z_i is achieved by adding and subtracting a charge distribution $-Z_i G_\sigma(\mathbf{r})$ around every position $\mathbf{r}_i$, where G_σ is a normalized Gaussian distribution with standard deviation σ. The interaction then splits into a short-range part, which can be computed in real space by a finite sum over a few unit cells, and a long-range term that has a fast-decaying analytical expression in reciprocal space. The standard deviation σ of the Gaussian is a tunable parameter that allows for balancing short- and long-range contributions and reasonably small cutoffs in both spaces. The Coulomb energy becomes[23,24]

$$\begin{aligned} U_{\mathrm{Coul}} &= U_S + U_L - U_{\mathrm{self}} \\ &= \frac{1}{4\pi\epsilon_0}\frac{1}{2}\sum_{i=1}^{N}\sum_{\mathbf{n}}\sum_{j=1}^{N}{}' \frac{\mathrm{Z_i Z_j}}{|\mathbf{r_i}-\mathbf{r_j}+\mathbf{R_n}|} \\ &\quad\times \mathrm{erfc}\left(\frac{|\mathbf{r_i}-\mathbf{r_j}+\mathbf{R_n}|}{\sqrt{2}\sigma}\right) + \frac{1}{2V_{\mathrm{prim}}\epsilon_0} \\ &\quad\times \sum_{\mathbf{G}\neq 0}\frac{\exp(-\sigma^2 G^2/2)}{G^2}|\mathcal{S}(\mathbf{G})|^2 \\ &\quad - \frac{1}{4\pi\epsilon_0}\frac{1}{\sqrt{2\pi}\sigma}\sum_{i=1}^{N} Z_i^2. \end{aligned} \tag{A1}$$

Here, $\mathbf{R_n} = n_1\mathbf{a}_1 + n_2\mathbf{a}_2 + n_3\mathbf{a}_3$ is a real-space lattice vector, $\mathbf{G} = n_{k1}\mathbf{b}_1 + n_{k2}\mathbf{b}_2 + n_{k3}\mathbf{b}_3$ is a reciprocal lattice vector, $\mathcal{S}(\mathbf{G}) \equiv \sum_i Z_i e^{i\mathbf{G}\mathbf{r}_i}$ is called structure factor, and $\mathrm{erfc(x)} \equiv 1 - \mathrm{erf(x)}$ is the complementary error function. We compute the sums using $\sigma = 0.05$ nm $\sim \frac{r_0}{5}$, with a cutoff in reciprocal space of $-5 \leqslant n_{ki} \leqslant 5$ and short-range interactions up to the second-nearest neighbor (cutoff range $\sim$0.3 nm).

The computation of contributions to the dynamical matrix arising from Eq. (A1) is nontrivial due to nonanalytical behavior at $\mathbf{q}=0$.[3,23] The results obtained in Ref. 23 are replicated here for completeness. The contribution to the dynamical matrix element $D_{i\mu,jv}(\mathbf{q})$ [where i,j are atom indices and $\mu,\nu \in \{x,y,z\}$, see Eq. (9)] arising from such Coulomb forces is

$$\begin{aligned} D^C_{i\mu,jv}(\mathbf{q}) &= -\frac{Z_i Z_j}{4\pi\epsilon_0\sqrt{M_i M_j}} Q_{\mu\nu}(i,j|\mathbf{q}) \\ &\quad + \delta_{ij}\sum_{j'}\frac{Z_i Z_{j'}}{4\pi\epsilon_0 M_i} Q_{\mu\nu}(i,j'|\mathbf{0}). \end{aligned} \tag{A2}$$

Here, δ_{ij} is the Kronecker symbol, V is the volume of the cell, and the index j' runs over all the atoms of the considered cell. $Q_{\mu\nu}(i,j|\mathbf{q})$ is defined as follows:

$$\begin{aligned} Q_{\mu\nu}(i,j|\mathbf{q}) &\equiv -\delta_{\mathbf{q}\neq 0}\frac{4\pi}{V}\frac{q_\mu q_\nu}{q^2} e^{-\sigma^2 q^2/2} e^{i\mathbf{q}\cdot(\mathbf{r}_i-\mathbf{r}_j)} \\ &\quad - \frac{4\pi}{V}\sum_{\mathbf{G}\neq 0}\frac{|\mathbf{G}+\mathbf{q}|_\mu |\mathbf{G}+\mathbf{q}|_\nu}{|\mathbf{G}+\mathbf{q}|^2} e^{-\sqrt{2}/4\sigma|\mathbf{G}+\mathbf{q}|^2} \\ &\quad\times e^{i(\mathbf{G}+\mathbf{q})\cdot(\mathbf{r}_i-\mathbf{r}_j)} + \frac{1}{(\sqrt{2}\sigma)^3}\sum_{\mathbf{n}} H_{\mu\nu} \\ &\quad\times \left(\frac{\mathbf{r}_i - \mathbf{r}_j + \mathbf{R_n}}{\sqrt{2}\sigma}\right) e^{-i\mathbf{q}\cdot(\mathbf{r}_i-\mathbf{r}_j+\mathbf{R_n})}. \end{aligned} \tag{A3}$$

The index $\mathbf{n}$ includes the primary cell itself. The function H is defined as

$$\begin{aligned} H_{\mu\nu}(\mathbf{x}) &\equiv \frac{x_\mu x_\nu}{x^2}\left[\frac{3}{x^3}\mathrm{erfc(x)} + \frac{2}{\sqrt{\pi}}\left(\frac{3}{\mathrm{x}^2}+2\right)\mathrm{e}^{-\mathrm{x}^2}\right] \\ &\quad - \delta_{\mu\nu}\left(\frac{1}{x^3}\mathrm{erfc(x)} + \frac{2}{\sqrt{\pi}}\frac{1}{\mathrm{x}^2}\mathrm{e}^{-\mathrm{x}^2}\right). \end{aligned} \tag{A4}$$

The sound velocities in Table II were computed from finite differences in the absence of the nonanalytic term on the first line of Eq. (A3). Inclusion of this term even for small $\mathbf{q}$ results in erroneous values, in particular, for $c_s^{\mathrm{TA2}}[110]$ and $c_s^{\mathrm{LA}}[111]$.

APPENDIX B: PARAMETER FITTING PROCEDURE

The parameter sets of Table I were found using a parallel genetic algorithm[50] (PGA) fitting method. This method is inspired and steered by biological processes. The fitting process starts with an initial population of random force constants, which are coded as chromosomes. By applying selection, crossover, and mutation processes to chromosomes, a better population is searched for. The measure of fitness is provided by a cost function, which is taken as the sum of the weighted least-square residuals between the target values and model outputs. The GA process tries to minimize this cost function. The algorithm is stopped after a fixed number of iterations.

The fitting was divided into two phases: In a first phase, the eight or five harmonic force constants α_0, β_0, γ_0, δ_0, and ν_0 were fitted against some or all branches of the dispersion relation, the sound velocities, and possibly the elastic constants. Then, for fixed harmonic force constants, the anharmonic correction parameters A_α, A_β, A_γ, A_δ, A_ν were fitted to the Grüneisen parameters.

Three issues needed to be considered in the process:

(1) A multiobjective cost function was used in order to obtain a variety of physical characteristics of the material. The process of assigning weights to the various targets is intricate and requires manual adjustment. Thus, any fit reflects decisions on the relative importance of the targets, which can be adjusted at will.

(2) Model inputs need to be constrained in order to retain their physical meaningfulness. This was achieved by adding a large penalty to the cost value when a parameter lies outside a certain range. The range consists of a maximum (soft-wall) boundary of 45 N/m for α without which the GA for the acoustic mode fits would have pushed up the optical branches to unphysically high values. For the P8/el and P8/C sets, the coefficients β, γ, and δ were restricted to have positive values for the cation and negative values for the anion, as ambiguities in the signs may exist in the model. The five-parameter coefficients were restricted to be non-negative.

(3) Errors in reported experimental values were initially accounted for by modifying the cost function to vanish within a certain range, typically 1%, of the target rather than just

the target itself. However, this adjustment did not improve the fitting process, and the reported parameter sets do not include this feature.

An evolutionary algorithm was employed due to the complexity of the cost function and multiobjective nature of the problem. To speed up the solution process, the PGA was run on eight cores simultaneously. Due to the randomness of the method, every optimization was performed 10 times and the best solution reported. More details about the process are given in Ref. 37.

*sebi.steiger@gmail.com

[1] M. Born and E. Bormann, Ann. Phys. (NY) **367**, 218 (1920).
[2] K. Rustagi and W. Weber, Solid State Commun. **18**, 673 (1976).
[3] P. Giannozzi, S. de Gironcoli, P. Pavone, and S. Baroni, Phys. Rev. B **43**, 7231 (1991).
[4] M. Musgrave and J. Pople, Proc. R. Soc. London, Ser. A **268**, 474 (1962).
[5] P. Keating, Phys. Rev. **145**, 637 (1966).
[6] O. Lazarenkova, P. Von Allmen, F. Oyafuso, S. Lee, and G. Klimeck, Superlattices Microstruct. **34**, 553 (2003).
[7] S. Lee, O. L. Lazarenkova, P. Von Allmen, F. Oyafuso, and G. Klimeck, Phys. Rev. B **70**, 125307 (2004).
[8] R. Martin, Phys. Rev. B **1**, 4005 (1970).
[9] H. Fu, V. Ozoliņš, and A. Zunger, Phys. Rev. B **59**, 2881 (1999).
[10] K. Biswas, A. Franceschetti, and S. Lany, Phys. Rev. B **78**, 85212 (2008).
[11] J. Zi, X. Wan, G. Wei, K. Zhang, and X. Xie, J. Phys. Condens. Matter **8**, 6323 (1996).
[12] H. McMurry, A. Solbrig Jr., and J. Boyter, J. Phys. Chem. Solids **28**, 2359 (1967).
[13] Z. Sui and I. P. Herman, Phys. Rev. B **48**, 17938 (1993).
[14] E. O. Kane, Phys. Rev. B **31**, 7865 (1985).
[15] A. J. Williamson, L. W. Wang, and A. Zunger, Phys. Rev. B **62**, 12963 (2000).
[16] K. Kim, P. R. C. Kent, A. Zunger, and C. B. Geller, Phys. Rev. B **66**, 45208 (2002).
[17] D. N. Talwar and M. Vandevyver, Phys. Rev. B **41**, 12129 (1990).
[18] A. Paul, M. Luisier, and G. Klimeck, J. Comput. Electron. **9**, 160 (2010).
[19] W. Harrison, *Elementary Electronic Structure* (World Scientific, Singapore, 2004).
[20] P. Yu and M. Cardona, *Fundamentals of Semiconductors* (Springer, Berlin, 2005).
[21] R. Martin, Phys. Rev. **186**, 871 (1969).
[22] W. Weber, Phys. Rev. B **15**, 4789 (1977).
[23] A. Maradudin, E. Montroll, G. Weiss, and I. Ipatova, *Theory of Lattice Dynamics in the Harmonic Approximation* (Academic, New York, 1963).
[24] H. Lee and W. Cai (unpublished).
[25] E. Kellermann, Philos. Trans. R. Soc. London A **238**, 513 (1940).
[26] K. Kunc, M. Balkanski, and M. A. Nusimovici, Phys. Rev. B **12**, 4346 (1975).
[27] K. Kunc, M. Balkanski, and M. Nusimovici, Phys. Status Solidi B **72**, 229 (1975).
[28] H. Rucker and M. Methfessel, Phys. Rev. B **52**, 11059 (1995).
[29] D. Vanderbilt, S. H. Taole, and S. Narasimhan, Phys. Rev. B **40**, 5657 (1989).
[30] F. Cerdeira, C. Buchenauer, F. Pollak, and M. Cardona, Phys. Rev. B **5**, 580 (1972).
[31] F. Grosse and J. Neugebauer, Phys. Rev. B **63**, 85207 (2001).
[32] M. Blackman, Philos. Mag. **3**, 831 (1958).
[33] A. Rajagopal and R. Srinivasan, Z. Phys. A **158**, 471 (1960).
[34] J. Vetelino and S. Mitra, Solid State Commun. **7**, 1181 (1969).
[35] S. Steiger, M. Povolotskyi, T. Kubis, H.-H. Park, and G. Klimeck, IEEE Trans. Nanotechnol. (to be published).
[36] S. Yamakawa, R. Akis, N. Faralli, M. Saraniti, and S. Goodnick, J. Phys. Condens. Matter **21**, 174206 (2009).
[37] M. Salmani-Jelodar, S. Steiger, A. Paul, and G. Klimeck, *IEEE Congress on Evolutionary Computation (CEC)* (IEEE, 2011), pp. 2429–2435.
[38] S. Adachi, *Properties of Group-IV, II-V and II-VI Semiconductors* (Wiley, New York, 2005).
[39] O. Madelung, U. Rössler, and M. E. Schulz [www.springermaterials.com].
[40] C. Cousins, L. Gerward, J. Olsen, B. Selsmark, B. Sheldon, and G. Webster, Semicond. Sci. Technol. **4**, 333 (1989).
[41] D. Strauch and B. Dorner, J. Phys. Condens. Matter **2**, 1457 (1990).
[42] R. Cottam and G. Saunders, J. Phys. C **6**, 2105 (1973).
[43] B. Weinstein and R. Zallen, *Light Scattering in Solids IV*, edited by M. Cardona and G. Guntherodt (Springer, New York, 1984).
[44] A. Debernardi and M. Cardona, Phys. Rev. B **54**, 11305 (1996).
[45] K. Kunc and R. M. Martin, Phys. Rev. B **24**, 2311 (1981).
[46] R. Eryigit and I. P. Herman, Phys. Rev. B **53**, 7775 (1996).
[47] P. N. Keating, Phys. Rev. **149**, 674 (1966).
[48] J. M. Skipp and D. J. Dunstan, Phys. Rev. B **69**, 054105 (2004).
[49] R. N. Thurston and K. Brugger, Phys. Rev. **133**, A1604 (1964).
[50] E. Cantú-Paz, Calculateurs Paralleles, Reseaux et Systems Repartis **10**, 141 (1998).